

RXTE Observations of MXB 0656–072

Thomas Dauser
supervised by Jörn Wilms

October 13, 2008

In this work I analyzed four outbursts of the transient X-ray binary MXB 0656–072 which were monitored by pointed *RXTE* observations. The outburst during fall 2003 to 2004 was almost a factor three higher in luminosity than the three smaller ones, which occurred between november 2007 and june 2008. A cyclotron resonant scattering feature (CRSF) was found in the spectra which was used to estimate the magnetic field of the neutron star as $B = 3.89_{-0.02}^{+0.02} \cdot 10^{12}$ G. Furthermore it is shown that there exists a difference in the dependence of the CRSF on the luminosity between the outbursts. Moreover it seems like there could be a change in the accretion mechanism from super-Eddington to sub-Eddington regime visible during the 2003/04 outburst. The critical luminosity of this effect could be enclosed between $L = 0.9 \cdot 10^{37}$ erg s⁻¹ and $L = 1.3 \cdot 10^{37}$ erg s⁻¹.

Contents

1	Introduction	2
1.1	Neutron Stars	2
1.2	Accretion	3
1.3	MXB 0656–072	4
2	Data Analysis	4
2.1	The Rossi X-Ray Timing Explorer (<i>RXTE</i>)	4
2.1.1	The Satellite	4
2.1.2	Instrumentation	4
2.2	Data Reduction	6
2.3	Model Fitting	6
3	Spectral Modeling	8
3.1	General Spectral Shape	8
3.2	Evolution of the CRSF	9
3.3	Results	9
4	Discussion	10
4.1	The Different Accretion Regimes	10
4.2	The Shape of the Different Outbursts	11
4.3	The Strength of the Magnetic Field	11
4.4	Comparison with other Transient Sources	12
5	Summary	13

1 Introduction

1.1 Neutron Stars

Neutron stars are one possible endstage of stellar evolution. Their mass is above the Chandrasekhar limit of $1.44 M_{\odot}$, i.e., the pressure from the degenerated electrons is not high enough to form a stable state and neutronizes electrons and protons (Kutner, 2003). This configuration forms the densest known objects ($\rho \sim 10^{14} \text{ g cm}^{-3}$), implying that no stable state exists above their upper mass limit which lies between 3 and $4 M_{\odot}$. With the given mass limits this results in a radius about 10–15 km.

Besides that they often have very strong magnetic fields. There exist several theories that try to explain this fact (for further information see Reisenegger 2008). The most common one uses the fact that all stars have magnetic fields during their lifetime and makes the rough estimation that the magnetic flux

$$\Phi = 4\pi R^2 B \tag{1}$$

remains constant, especially during the death of the star. This gives a magnetic field of the

neutron star of

$$B_{\text{NS}} = \left(\frac{R_{\text{star}}}{R_{\text{NS}}} \right)^2 B_{\text{star}} \quad (2)$$

Since the typical radii of stars are about $5 \cdot 10^4$ times that of a neutron star it is possible that the B -fields can reach up to 10^{15} G (Grämer, 2008).

Neutron stars are classified by three main groups, the magnetars, the radio pulsars and the X-ray binaries. According to the mass of their companion star the last group is divided into the High Mass X-Ray Binaries (HMXB) and the Low Mass X-Ray Binaries (LMXB). As the source I will analyze is a HMXB, I will focus on the special features of this class of binaries.

1.2 Accretion

One mechanism linked very closely to neutron stars in binary systems is accretion (for detailed information see Fröhlich 2003). This process implies that mass from the companion star falls into the deep gravitational potential of the neutron star, which frees over 20 times more energy than the fusion from hydrogen to helium of the same mass (Grämer, 2008). The matter of the

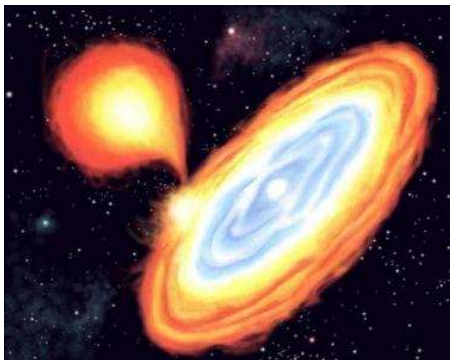


Figure 1: An illustration of the Roche-Lobe-Accretion.¹

companion star can reach the compact object in different ways. If the star is larger than its Roche Lobe, matter can flow over the inner Lagrangian-Point between the two objects towards the neutron star, form an accretion disc and fall onto its surface (see Fig. 1). This process, which is called Roche Lobe overflow, is the dominant accretion mechanism in LMXBs. In HMXB there can be also accretion of matter which was blown away as stellar wind, if the binary partner is an O or B star and the distance between the two objects is small enough. One last possibility is the so called Be-Mechanism, named after extra emission lines in the optical spectrum of companion that come from a disc around it. To accrete material in such a system, the neutron star has to be in an eccentric orbit that brings it at some time of its orbit very close or into this disc. At this time, the mass transfer rate is so high that it comes to an outburst, which can last from a few days up to months. This transient behavior also implies that for most of the time these compact objects have very weak luminosities.

¹Source: [http:// www.sciencedaily.com/releases/2007/04/070413111509.htm](http://www.sciencedaily.com/releases/2007/04/070413111509.htm)

1.3 MXB 0656–072

The neutron star MXB 0656–072 was categorized as a Low Mass X-Ray Binary for almost 30 years (Kaluziński, 1976) until an outburst in 2003 was monitored which reached an X-Ray luminosity of 200 mCrab (Remillard & Marshall, 2003). Their observation led to the new classification as a transient High Mass X-Ray Binary with an O9.7Ve companion star and a pulse period of 160.7s (McBride et al., 2006). The distance to the object is estimated by McBride et al. (2006) to 3.9 ± 0.1 kpc.

Heindl et al. (2003) and McBride et al. (2006) showed that a cyclotron resonance scattering feature (later called CRSF or just 'cyclotron line') at ~ 34 keV is present in the spectrum. This means that the magnetic field is strong enough that the electrons of the in-falling matter circle in such small radii around the B -field lines that one has to take quantum mechanical effects into account. Theory shows that the electron energies are quantized in so-called Landau-Levels ($n = 1, 2, 3, \dots$), allowing absorption (more precisely: resonance scattering) features at the energy

$$E_c \sim 11.57 \text{ keV} \cdot \frac{B}{10^{12} \text{ G}} \cdot n \quad (3)$$

depending on the magnetic field B (Schönherr et al., 2007). Taking the gravitational redshift z into account the observed energy of the fundamental line ($n = 1$) shifts approximately to

$$E_c^{\text{obs}} \sim 11.57 \text{ keV} \cdot \frac{1}{1+z} \cdot \frac{B}{10^{12} \text{ G}} \quad (4)$$

(McBride et al., 2006).

2 Data Analysis

2.1 The Rossi X-Ray Timing Explorer (RXTE)

2.1.1 The Satellite

The data used for the analysis were obtained with the Rossi X-Ray Timing Explorer (*RXTE*), a NASA satellite designed to study especially the time variability of X-ray sources. Since its launch on 1995 December 30, it orbits the Earth every 90 minutes. Fig. 2 shows a sketch of the spacecraft and its principal components. Equipped with a full three-axis momentum wheel system it can turn at the high rate of 12° per minute and is therefore able to reach every observable coordinate in a short period of time (Giles et al., 1995).

2.1.2 Instrumentation

RXTE is equipped with three instruments (Fig. 2), the Proportional Counter Array (PCA), the High Energy X-Ray Timing Experiment (HEXTE) and the All-Sky Monitor (ASM). Detailed information on the whole spacecraft can be found in Bradt et al. (1990) and Giles et al. (1995). This section is based on these two references. More facts to the single instruments are depicted by Rothschild et al. (1998), Gruber et al. (1996) and Jahoda et al. (2006).

²Source: http://heasarc.gsfc.nasa.gov/docs/xte/xte_images.html

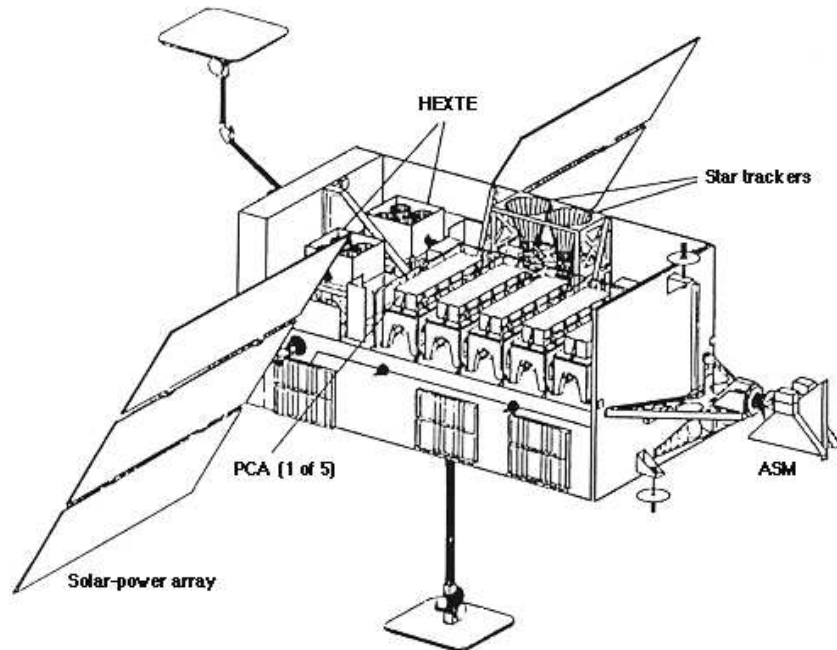


Figure 2: A sketch of the *RXTE* spacecraft with its basic components.²

The **ASM** (see Fig. 2) covers an energy spectrum from 2 to 10 keV and is designed to monitor most of the sky every day and watch for irregularities in the arriving flux. This is achieved by three separated coded-mask imaging detectors placed offset, which are able to rotate in order to have a maximum field of view while PCA and HEXTE perform pointed observations. Taking into account the different orientations of *RXTE* due to observations of different sources each day it is possible to scan the whole X-ray sky above ~ 10 mCrab (~ 75 sources). The results are available immediately which can be used to direct the spacecraft to a position where the All-Sky Monitor detects irregularities in the arriving flux, e.g., if a transient source like MXB 0656–072 starts its outburst.

The whole satellite has to rotate if the two other detectors are directed towards the desired source, because they are fixed on *RXTE* and coaligned, too, to monitor the same source at the same time. **PCA** (see Fig. 2) consists of five conventional proportional counters filled mostly with Xe gas and has an energy range of 2–60 keV. Additionally, a microprocessor system with several modes allows a time resolved study up to a resolution of $1 \mu\text{s}$.

HEXTE (see Fig. 2) completes the features of the *RXTE* by extending the upper energy range to 250 keV. But it also can detect photons down to energies about 20 keV which creates an overlap with the PCA energy range. This capability can be used for reliable cross-calibration between the two detectors. In order to achieve such an energy range the experiment is arranged in two clusters, each consisting of four NaI/CaI phoswich scintillators (see Fig. 3 for a schematic picture). These clusters have the special feature that they can be 'rocked' on or off the source every 16 s with their rotating axes aligned orthogonally. This arrangement provides an accurate monitoring of the background, as one set of detectors is directed at the source while the other

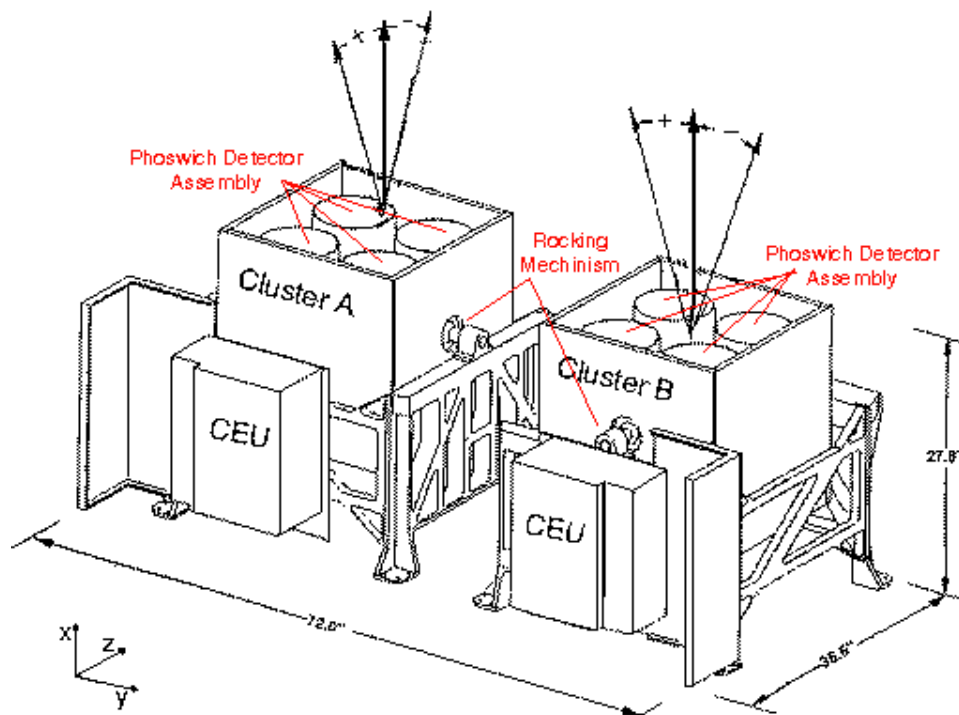


Figure 3: Schematic draw of the 'rocking' HEXTE.³

measures the background at the same time.

2.2 Data Reduction

RXTE monitored the source with PCA and HEXTE over the large outburst from fall 2003 to spring 2004 and three smaller ones from november 2007 to june 2008. Fig. 4 shows the measured flux over the outbursts observed by ASM. Each triangle indicates one observation of the two detectors.

Having looked at different spectra I decided to trust the values of PCA from 4 to 22 keV and following McBride et al. (2006), added a systematic error of 0.5% to the data in order to take the uncertainties in the response matrix into account.

Given that the average luminosity of the source is comparably weak, I rebinned the HEXTE data with the criteria of a signal to noise ratio of 3 : 1. This approach set the upper limit of the energy range, depending on the flux, between 35 and 100 keV.

2.3 Model Fitting

For the models and the fitting I used the software ISIS (for further details on ISIS see Houck & Denicola 2000). The calculation of the confidence intervals was done by the PVM-modul of ISIS requiring 90 % uncertainty.

³Source: http://mamacass.ucsd.edu/hexite/pictures/hexite_clusters_3d_sm1.gif

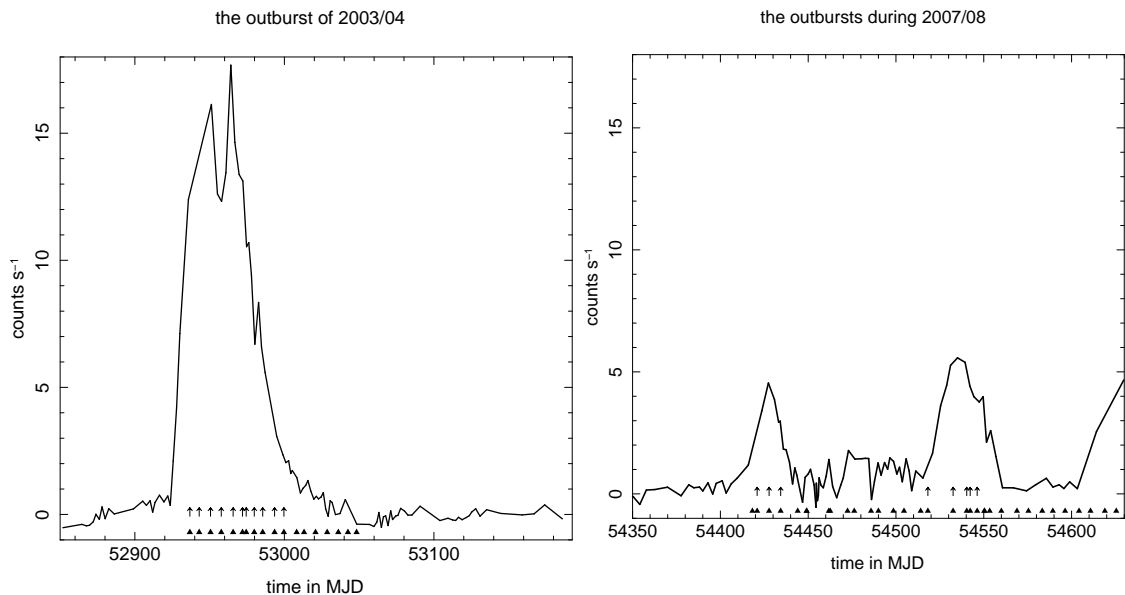


Figure 4: The large outburst from fall 2003 to spring 2004 and the three smaller ones from november 2007 to june 2008 monitored by ASM. Each triangle indicates one pointed observation of PCA and HEXTE. The measurements marked by the arrows are selected by special requirements in HEXTE exposure and flux described in Sec. 3.2.

After analyzing a few spectra it was found that the model

$$\text{CONT}(E) = \begin{cases} 1 & \text{for } E < E_{\text{cut}} \\ e^{\frac{E-E_{\text{cut}}}{E_{\text{fold}}}} & \text{for } E \geq E_{\text{cut}} \end{cases} \quad (5)$$

describes the continuum best. Following McBride et al. (2006) I added a Gaussian shaped emission feature to smooth the cutoff. For acceptable χ^2 values I also had to take models for a black body (*BBODY*) and photoabsorption (*PHABS*) into account. Furthermore a strong Fe emission line is present in the spectrum at ~ 6.4 keV which is described by the Gaussian shaped model *EGAUSS*. As stated by McBride et al. (2006) I found a systematic feature at ~ 10 keV in the spectrum that I modeled with the *GABS*-function of ISIS. For further details on this feature which could be observed at different sources (Her X-1, GS 1843+00) see Coburn (2001). For modelling the CRSF I used a Lorentzian shape as implemented in the *CYCLABS*-function.

$$\text{CYCLABS}(E) = \exp \left(-D_c \frac{\left(\frac{W_c E}{E_c} \right)^2}{(E - E_c)^2 + W_c^2} \right) \quad (6)$$

The upper panel in Fig. 5 shows the complete model and the two lower ones make it obvious that adding a CRSF is necessary in order to describe the incoming flux. The well visible feature at ~ 6.4 keV is interpreted as the Fe emission feature mentioned above.

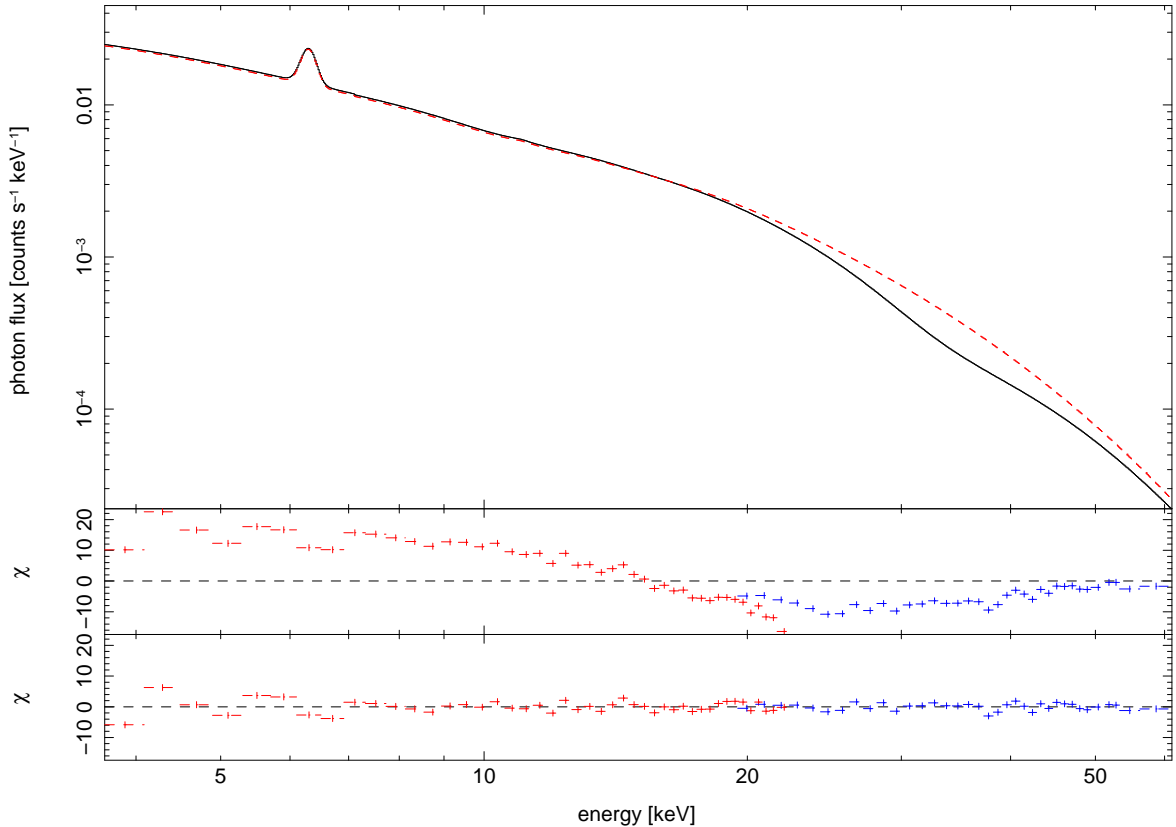


Figure 5: The model to the spectrum of MXB 0656–072 on 2003-11-23. The dashed line (corresponding residuals in the second panel) describes the model without the cyclotron line, which has been renormalized ($\chi_{\text{red}}^2 = 34.6$). The solid line and the lower panel show the complete model, this time including the CRSF ($\chi_{\text{red}}^2 = 1.15$).

3 Spectral Modeling

3.1 General Spectral Shape

At first I fitted single spectra by hand and noticed that if the flux (calculated in the range of 4–50 keV) drops below $0.05 \text{ photons s}^{-1}$ or the exposure time falls below 1 ksec I could not detect any CRSF. The reason is the low signal to noise ratio, especially in the higher energy range of HEXTE, where the fundamental cyclotron line should be located.

To improve the signal to noise ratio I tried to add certain spectra. As I assumed a dependence on the flux I wrote an algorithm which fits all available spectra to acceptable χ^2 -values. With these models I could now estimate the averaged flux of each observation in order to select different spectra with similar flux and add them. I decided to add all observations below $0.17 \text{ photons s}^{-1}$, from 0.17 to $0.3 \text{ photons s}^{-1}$ and above $0.3 \text{ photons s}^{-1}$. The general results confirm the parameter values of McBride et al. (2006) and can be seen in Tab. 1, which has been divided into the three spectra according to the flux Φ in units of photons s^{-1}

Table 1: Parameter values of combined spectra of all available data, divided per flux as given in the table. The confidence intervals are at the 90 % uncertainty level.

Parameter	$\Phi < 0.17$	$0.17 < \Phi < 0.3$	$\Phi > 0.3$
χ_{red}^2	1.76	1.29	2.03
Γ (photon index)	$1.025^{+0.001}_{-0.069}$	$0.95^{+0.04}_{-0.06}$	$0.763^{+0.001}_{-0.001}$
E_{cut} in keV	$11.92^{+0.08}_{-0.02}$	$11.8^{+0.6}_{-0.8}$	$11.46^{+0.01}_{-0.01}$
E_{fold} in keV	$12.40^{+0.01}_{-0.04}$	$11.3^{+0.2}_{-0.9}$	$11.22^{+0.01}_{-0.01}$
T_{body} in keV	$1.27^{+0.07}_{-0.14}$	$0.78^{+0.81}_{-0.18}$	$0.90^{+0.01}_{-0.07}$
N_{H} in 10^{22} cm^{-2}	$0.89^{+0.08}_{-0.11}$	$1.5^{+2.2}_{-1.5}$	$1.10^{+0.07}_{-0.07}$
E_{CRSF} in keV	$31.3^{+0.4}_{-1.2}$	$32.6^{+0.6}_{-1.0}$	$32.86^{+0.04}_{-0.04}$
W_{CRSF} in keV	$8.3^{+0.2}_{-0.8}$	$7.7^{+3.3}_{-2.1}$	$12.9^{+0.1}_{-0.1}$
D_{CRSF} in keV	$0.42^{+0.01}_{-0.06}$	$0.37^{+0.04}_{-0.05}$	$0.427^{+0.002}_{-0.002}$

3.2 Evolution of the CRSF

Despite all efforts not all fits resulted in low χ^2 -values which led me to the conclusion that different things might happen in the outbursts. This fact was encouraged by the strange evolution of some parameters like Γ or E_{CRSF} (see Tab. 1) which did not allow any plausible interpretation of the dependence on the flux.

In order to analyze the variation of the cyclotron line with the flux I fitted the single spectra again, but with a few restrictions. At first I only considered observations with $\Phi > 0.05 \text{ photons s}^{-1}$ and HEXTE exposure $t_{\text{exp}} > 1 \text{ ksec}$ to get reliable parameters (selected observations indicated by the arrows in Fig. 4). Furthermore I developed an algorithm for fitting, which froze (photoabsorption N_{H}) or constricted (photon index Γ , E_{cut} and E_{fold}) the parameters of the continuum and added the CRSF as last step. The photoabsorption was fixed at $N_{\text{H}} = 7.28 \cdot 10^{21} \text{ cm}^{-2}$ in analogy with McBride et al. (2006), which is estimated from the column density in direction of the source. The other parameters were defined by the combined spectra with flux $\Phi > 0.3 \text{ photons s}^{-1}$ (see Sec. 3.1). For the confidence interval calculation with PVM the whole continuum except for the *BBODY* remained frozen.

3.3 Results

The results of the analysis of the luminosity related change of the CRSF described in Sec. 3.2 are displayed in Fig. 6. In order to compare this with results from other transient sources like presented by Mihara et al. (2007) I plotted the luminosity instead of the flux. It was calculated by integrating over the unabsorbed model flux from 0.1 to 100 keV and using the distance $d = 3.9 \text{ kpc}$ estimated by McBride et al. (2006). I fitted the additional lines by minimizing the square-distance (linear regression) in respect to the error. They indicate the direction in which the CRSF position evolves.

During the outbursts of 2007/08, the cyclotron line energy does not shift significantly which

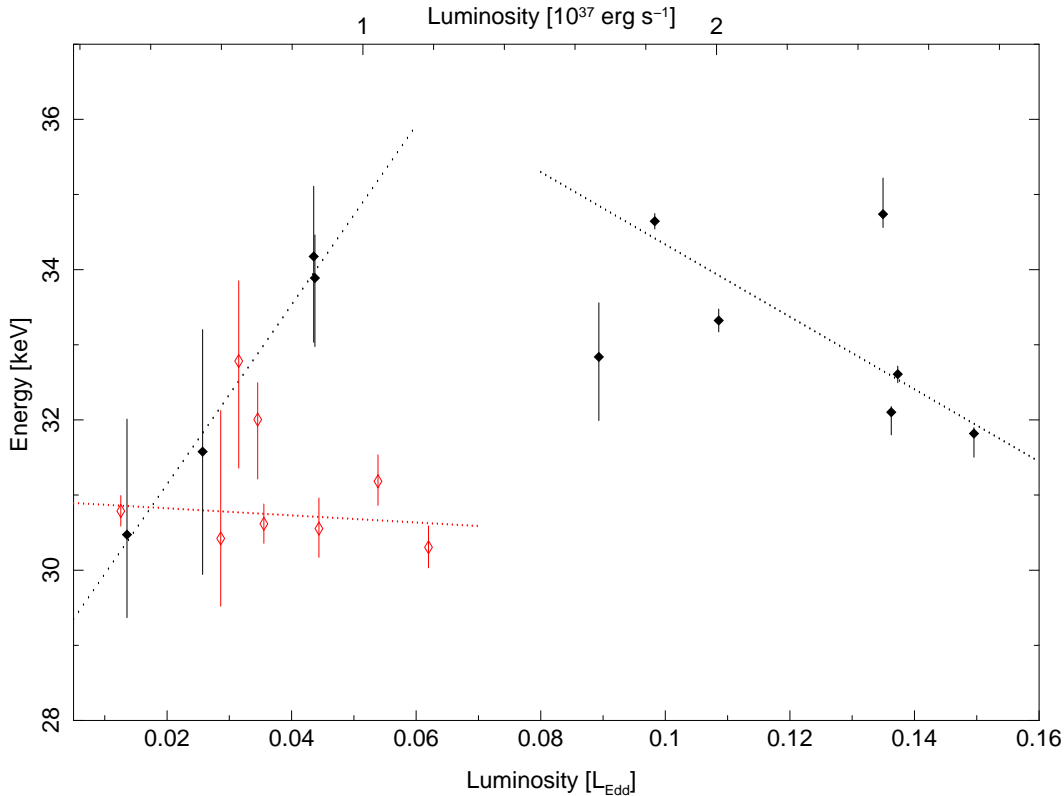


Figure 6: The fundamental cyclotron line of all spectra with $\Phi > 0.05 \text{ photons s}^{-1}$ and HEXTE exposure $t_{\text{exp}} > 1 \text{ ksec}$ is plotted against the luminosity. The filled diamonds depict observations of the huge 2003/04 outburst and the empty diamonds are from the outbursts of 2007/08. By using linear regression, the dotted lines were calculated in order to indicate the assumed direction of the variation.

is shown by the dotted red line I fitted through these points in Fig. 6. By contrast the CRSF energy during the outburst in 2003/04 varies from $34.7^{+0.5}_{-0.2} \text{ keV}$ to $31.6^{+1.6}_{-1.6} \text{ keV}$. Furthermore in the lower part ($L/L_{\text{Edd}} < 0.05$), the line energy rises with higher luminosities whereas for $L/L_{\text{Edd}} > 0.09$ the correlation is inverted and the CRSF position declines. For a better visibility of this I fitted two lines, one for each part, to emphasize the correlation depending on the luminosity.

4 Discussion

4.1 The Different Accretion Regimes

Fig. 6 shows two different correlations between luminosity and CRSF for the outburst of 2003/04. As the fundamental cyclotron line is directly correlated to the magnetic field (see Sec. 1.3) and the luminosity to the accretion rate, there has to be a change in the correlation

between the B -field and the accretion mechanism, or to be more precise, the structure of the accretion column has to change. This change takes place at a certain critical luminosity L_C (Nelson et al., 1993).

In the super-Eddington regime ($L > L_C$, right black line in Fig. 6) the height of the shock front above the neutron star (where the cyclotron resonant scattering takes place) increases with luminosity, which means that the magnetic field for this region, and therefore the cyclotron line energy, drops (Burnard et al., 1991).

On the other hand in the sub-Eddington regime ($L < L_C$, left black line in Fig. 6) no shock is forming because the accretion rate is not high enough to prevent the photons from leaving. For this regime Staubert et al. (2007) estimate the correlation of the height of the emission region above the neutron star with the accretion rate \dot{M} . They calculated that if the luminosity increases by a factor of two the energy changes like $\Delta E_C/E_C \simeq 0.03$. Estimating this correlation for the 2003/04 outburst with the fitted line, I obtained a ratio of $\Delta E_C/E_C \sim 0.10$. Considering that the line was fitted through only four points with large uncertainty and that – according to Staubert et al. (2007) – the local \dot{M} does not have to be exactly proportional to the observed luminosities, this interpretation is a possible explanation. Unfortunately there exists a gap in the available data for luminosities where the change from sub- to super-Eddington regime could take place, which prevents a more detailed analysis of this feature. But by looking at Fig. 6 the critical luminosity L_C can be enclosed somewhere between $0.9 \cdot 10^{37} \text{ erg s}^{-1}$ and $1.3 \cdot 10^{37} \text{ erg s}^{-1}$.

4.2 The Shape of the Different Outbursts

As already mentioned in Sec. 3.3, the outburst of 2003/04 obviously differs in its behavior from the smaller ones during 2007/08 (see Fig. 6). The 2003/04 outburst shows two different dependencies of the cyclotron line energy on luminosity (see Sec. 4.1), whereas almost no correlation could be observed for the smaller outbursts.

My interpretation of Fig. 6 according to this change is that the peaks of the outburst (indicated by the red rectangles and the filled black rectangles associated with the right black line) can be both described by the super-Eddington accretion mechanism. The four observations fitted with the left black line are situated in the decline (1/3 to 1/8 of the maximum luminosity) of the outburst. As explained in Sec. 4.1, the variation of the CRSF position in this direction can be described by the model for the sub-Eddington regime and is consistent with theory. Thus the source behaves different in the decline than at the peak of the outburst.

4.3 The Strength of the Magnetic Field

The strength of the B -field can easily be calculated by

$$B = \frac{1+z}{11.6 \text{ keV}} \cdot E_C^{\text{obs}} \cdot 10^{12} \text{ G} \quad (7)$$

(see Sec. 1.3) and assuming a gravitational redshift of $z = 0.3$ which is estimated for a common neutron star (McBride et al., 2006). The highest line energy is taken for the calculation, because this is when the cyclotron resonant scattering is closest to the surface of the neutron star (see Sec. 4.1) and therefore the B -field closest to its origin. With the assumption that the

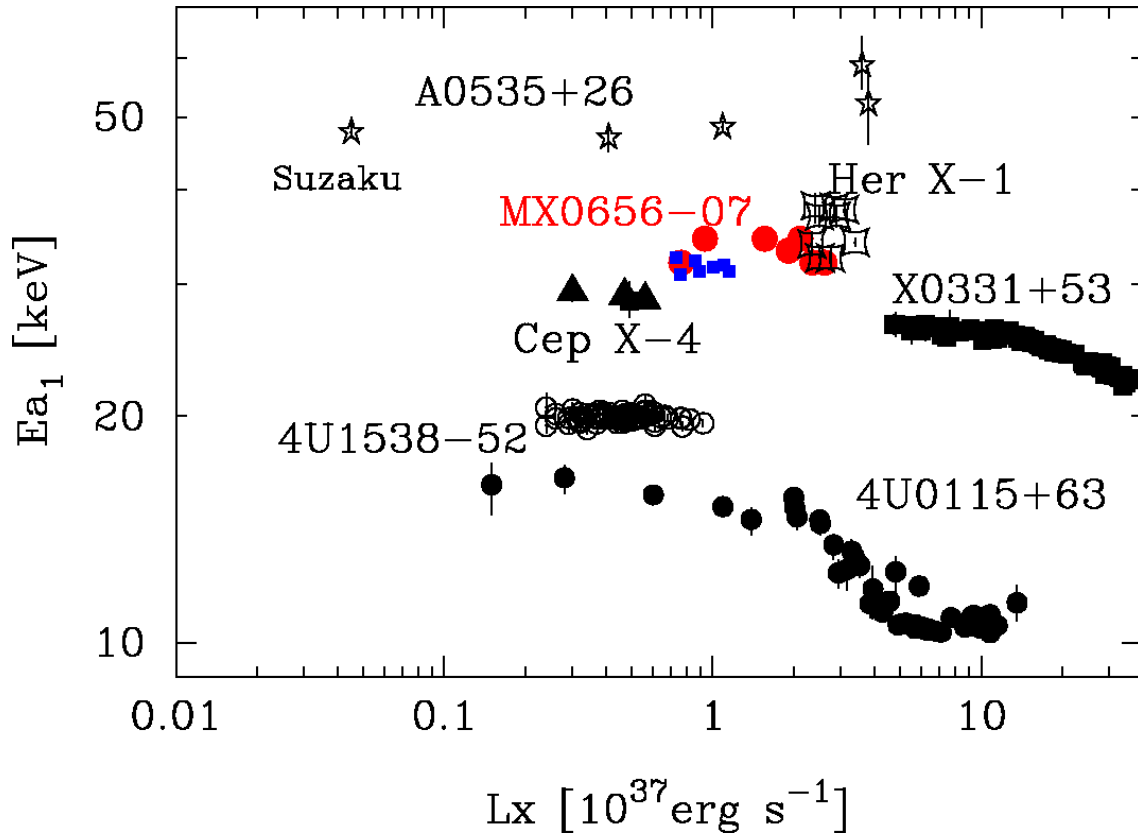


Figure 7: Edited plot by Mihara et al. (2007) in which I replaced the values of MXB 0656–072 with the ones I derived. The red circles are the observations of the 2003/04 outburst and the blue rectangles are taken from the smaller outburst during 2007/08.

observed line is the fundamental CRSF, situated at $E_{\max} = 34.7^{+0.5}_{-0.2}$ keV, the magnetic field is estimated to be $B = 3.89^{+0.06}_{-0.02} \cdot 10^{12}$ G. This value is slightly above the one McBride et al. (2006) calculated. Considering that they derived this by adding all spectra of the 2003/04 outburst it is convincing that I get a higher value by picking the single spectra with the lowest accretion column.

4.4 Comparison with other Transient Sources

Mihara et al. (2007) plotted the fundamental cyclotron line energy for several known transient sources over the luminosity. In Fig. 7 I edited this plot by replacing the values for MXB 0656–072 with the ones I derived, separating the different outbursts (see Section 4.1). As the position of each dot I added is just a rough estimation, the evolution compared to other sources cannot be analyzed in detail with this plot. But it can be seen as an evidence that in general the values of this analysis fit well into the context of the other sources.

5 Summary

In this work I analyzed outbursts from 2003 up to now of MXB 0656–072, which were monitored by *RXTE*. The main results obtained are the following:

- A powerlaw with a high energy cutoff was deduced to be the best model for the continuum. It was improved by adding a Fe emission feature, photoabsorption and a blackbody.
- By analyzing single spectra it was found that a detection of the CRSF below a flux of $0.05 \text{ photons s}^{-1}$ is not possible.
- Adding spectra of similar flux of all outbursts could confirm the parameters obtained by McBride et al. (2006) in general, but led to strange evolutions of some parameters like Γ in detail. This was interpreted as an evidence that the outbursts differ from each other.
- For the outburst in 2003/04 it was found that the correlation of the cyclotron line energy and luminosity changes, which was interpreted as a change of the accretion mechanism from super-Eddington to sub-Eddington regime. This effect is depending on luminosity and be enclosed as occurring between $0.9 \cdot 10^{37} \text{ ergs}^{-1}$ and $1.3 \cdot 10^{37} \text{ ergs}^{-1}$.
- During the outbursts of 2007/08 the CRSF position showed almost no variability.
- The B -field was estimated to be $3.89_{-0.02}^{+0.06} \cdot 10^{12} \text{ G}$, using the highest cyclotron line energy for the calculation.

References

- Bradt H.V., Swank J.H., Rothschild R.E., 1990, *Advances in Space Research* 10, 297
- Burnard D.J., Arons J., Klein R.I., 1991, *apj* 367, 575
- Coburn W., 2001, Ph.D. thesis, AA(UNIVERSITY OF CALIFORNIA, SAN DIEGO)
- Fröhlich H.E., 2003, *Sterne und Weltraum* 42
- Giles A.B., Jahoda K., Swank J.H., Zhang W., 1995, *Publications of the Astronomical Society of Australia* 12, 219
- Grämer C., 2008, *Zyklotronlinien – eine RXTE-Sample*, Zulassungsarbeit an der Dr. Remeis-Sternwarte Bamberg
- Gruber D.E., Blanco P.R., Heindl W.A., et al., 1996 120, C641
- Heindl W., Coburn W., Kreykenbohm I., Wilms J., 2003, *The Astronomer's Telegram* 200, 1
- Houck J.C., Denicola L.A., 2000, In: Manset N., Veillet C., Crabtree D. (eds.) *Astronomical Data Analysis Software and Systems IX*. ASP Conf. Ser. 216, p. 591
- Jahoda K., Markwardt C.B., Radeva Y., et al., 2006, *apjs* 163, 401

References

- Kaluzienski L.J., 1976, IAU Circ 2935
- Kutner M.L., 2003
- McBride V.A., Wilms J., Coe M.J., et al., 2006 451, 267
- Mihara T., Terada Y., Nakajima M., et al., 2007, Progress of Theoretical Physics Supplement 169, 191
- Nelson R.W., Salpeter E.E., Wasserman I., 1993, apj 418, 874
- Reisenegger A., 2008, ArXiv e-prints
- Remillard R., Marshall F., 2003, The Astronomer's Telegram 197
- Rothschild R.E., Blanco P.R., Gruber D.E., et al., 1998, ApJ 496, 538
- Schönherr G., Wilms J., Kretschmar P., et al., 2007, A&A 472, 353
- Staubert R., Shakura N.I., Postnov K., et al., 2007 465, L25